Betzler, C., Eberli, G.P., Alvarez Zarikian, C.A., and the Expedition 359 Scientists
Proceedings of the International Ocean Discovery Program Volume 359
publications.iodp.org

doi:10.14379/iodp.proc.359.107.2017

Site U1469[1]

C. Betzler, G.P. Eberli, C.A. Alvarez Zarikian, M. Alonso-García, O.M. Bialik, C.L. Blättler, J.A. Guo, S. Haffen, S. Horozal, M. Inoue, L. Jovane, D. Kroon, L. Lanci, J.C. Laya, A. Ling Hui Mee, T. Lüdmann, M. Nakakuni, B.N. Nath, K. Niino, L.M. Petruny, S.D. Pratiwi, J.J.G. Reijmer, J. Reolid, A.L. Slagle, C.R. Sloss, X. Su, P.K. Swart, J.D. Wright, Z. Yao, and J.R. Young[2]

Keywords: International Ocean Discovery Program, IODP, *JOIDES Resolution*, Expedition 359, Site U1469, Maldives, Kardiva Channel, Goidhoo atoll, Indian Ocean paleoceanography, Oligocene, Miocene, Pliocene, Pleistocene, carbonate platform, carbonate platform drowning, celestine, dolomite, drift deposits, large benthic foraminifers, monsoon, sea level, sequence stratigraphy

Contents

Background and objectives

Site U1469 (proposed Site MAL-08A) lies 2.87 km (1.57 nmi) south-southwest of Site U1465, which is the westernmost site of the northern transect in the western part of the Kardiva Channel (Figure F1). It is located at 4°54.41′N, 73°0.49′E, at a water depth of 432 m. The site was selected to document and reconstruct the carbonate bank depositional system of the drowned Miocene bank and to

Figure F1. Location map of Site U1469, located in the Kardiva Channel just north of the northeastern corner of Goidhoo atoll at 432 m water depth.

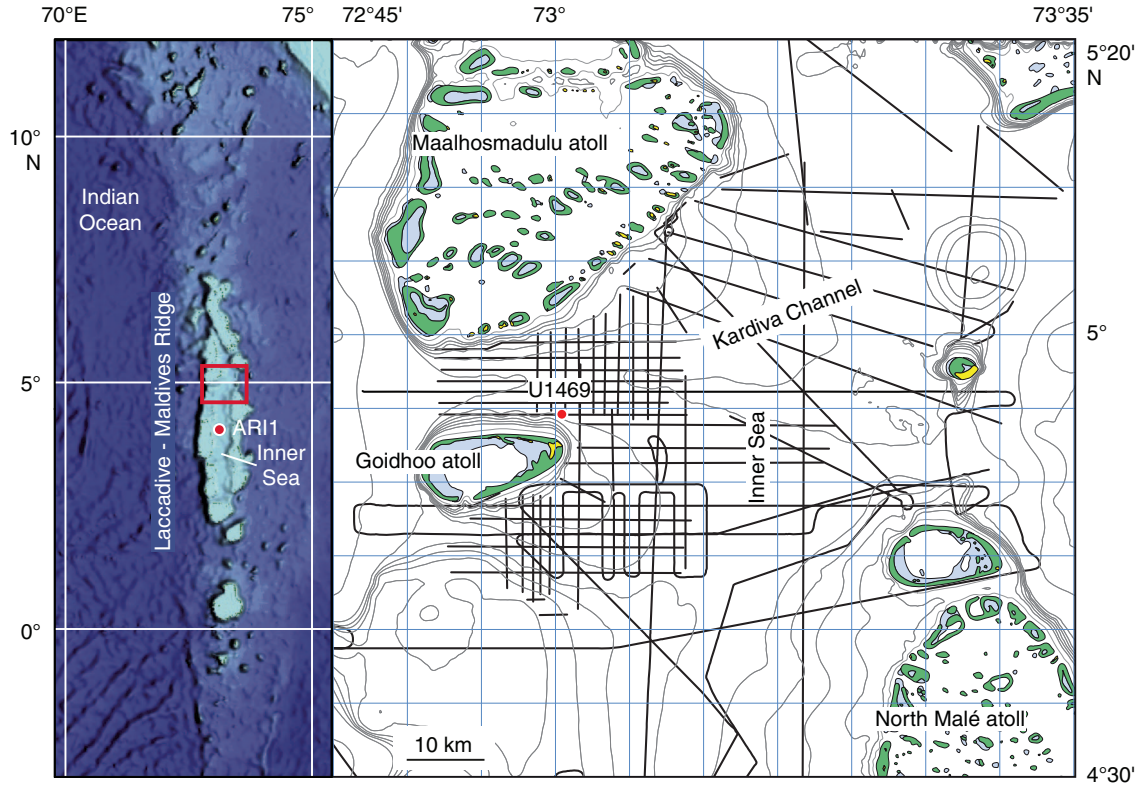

[1] Betzler, C., Eberli, G.P., Alvarez Zarikian, C.A., Alonso-García, M., Bialik, O.M., Blättler, C.L., Guo, J.A., Haffen, S., Horozal, S., Inoue, M., Jovane, L., Kroon, D., Lanci, L., Laya, J.C., Ling Hui Mee, A., Lüdmann, T., Nakakuni, M., Nath, B.N., Niino, K., Petruny, L.M., Pratiwi, S.D., Reijmer, J.J.G., Reolid, J., Slagle, A.L., Sloss, C.R., Su, X., Swart, P.K., Wright, J.D., Yao, Z., and Young, J.R., 2017. Site U1469. *In* Betzler, C., Eberli, G.P., Alvarez Zarikian, C.A., and the Expedition 359 Scientists, *Maldives Monsoon and Sea Level*. Proceedings of the International Ocean Discovery Program, 359: College Station, TX (International Ocean Discovery Program). http://dx.doi.org/10.14379/iodp.proc.359.107.2017

[2] **Expedition 359 Scientists' addresses.**

MS 359-107: Published 4 May 2017

link the seismic sequences to facies. This link is possible because the drowning unconformity does not mask underlying geometries at this site. The seismic section of Site U1469 images the drowned Kardiva platform overlain by nearly transparent seismic facies of the current-dominated sheeted drift. The seascape at the modern seafloor contains large sand waves seen on the seismic data as short irregular reflections (Figure **F16**). The target depth was 700 meters below seafloor (mbsf), the base of platform sequence (PS) PS7, which is the first sequence after the Kardiva platform went from mostly aggrading growth to progradation.

The specific objectives of Site U1469 were (1) to provide a detailed reconstruction of the predrowning, drowning, and postdrowning evolution of the carbonate bank by linking the seismic stratigraphic record to the sedimentary record (i.e., depositional facies); (2) to constrain the timing of this evolution, thus allowing age assignments of unconformities, sedimentary interruptions, sedimentary turnovers, and onset of drift deposition; and (3) to reconstruct and date bank to drift turnover. Sequences are characterized by mound-shaped reflection bundles manifested at the offlap break.

Operations

Transit to Site U1469

Site U1469 was only a 4 nmi transit from Site U1468, so the dynamic positioning system was used to move the ship to the new coordinates. During the transit, the drill string was recovered, and a new rotary core barrel (RCB) bottom-hole assembly (BHA) was assembled and lowered to the seafloor.

Hole U1469A

We tagged the seafloor with the drill bit and established a seafloor depth of 427 meters below sea level (mbsl). RCB coring in Hole U1469A started at 1825 h on 13 November 2015. Coring was extremely challenging because of the loosely cemented carbonate sand formation. High torque and overpull occurred when pulling the bit off the bottom of the hole. However, we were able to penetrate to 122.1 mbsf before making a wiper trip up. At 0245 h on 14 November, with the bit back on bottom again, RCB coring continued, but hole conditions continued to be problematic. We suspected that drilling had encountered a zone of high permeability within the buried reefal carbonate rocks, causing loss of circulation uphole that was required to clean the drilled cuttings off the hole. At 0630 h, we decided to abandon Hole U1469A and try a new hole after offsetting the ship 40 m west. The drill string was pulled clear of the seafloor at 0810 h on 14 November, ending Hole U1469A. Total core recovered in Hole U1469A was 4.14 m (3%). All 17 cores recovered were RCB cores (Table **T1**; see Figure **F1** in the Expedition 359 summary chapter [Betzler et al., 2017b]).

Hole U1469B

Drilling in Hole U1469B started at 0850 h on 14 November 2015 after using the drill bit to tag the seafloor (427 mbsl). Hole U1469B was drilled without coring to 122 mbsf without incident, and it ap-

Table T1. Site U1469 core summary. DRF = drilling depth below rig floor, DSF = drilling depth below seafloor, CSF = core depth below seafloor. NA = not applicable. H = advanced piston corer, F = half-length advanced piston corer, X = extended core barrel, R = rotary core barrel, numeric core type = drilled interval. (Continued on next page.) **Download table in .csv format.**

Hole U1469A
Latitude: 4°54.4143′N
Longitude: 073°0.410′E
Water depth (m): 426.93
Date started (UTC): 0625 h; 13 November 2015
Date finished (UTC): 0310 h; 14 November 2015
Time on hole (days): 0.86
Seafloor depth DRF (m): 438.0
Rig floor to sea level (m): 11.07
Penetration DSF (m): 161.1
Cored interval (m): 161.1
Recovered length (m): 4.14
Recovery (%): 2
Drilled interval (m): NA
Drilled interval (no.): 0
Total cores (no.): 17
RCB cores (no.): 17

Hole U1469B
Latitude: 4°54.4166′N
Longitude: 073°0.4694′E
Water depth (m): 426.91
Date started (UTC): 0310 h; 14 November 2015
Date finished (UTC): 1548 h; 14 November 2015
Time on hole (days): 0.53
Seafloor depth DRF (m): 438
Rig floor to sea level (m): 11.09
Penetration DSF (m): 151.4
Cored interval (m): 29.4
Recovered length (m): 0.72
Recovery (%): 2
Drilled interval (m): 122
Drilled interval (no.): 1
Total cores (no.): 3
RCB cores (no.): 3

Core	Top of cored interval DSF (m)	Bottom of cored interval DSF (m)	Interval advanced (m)	Recovered length (m)	Curated length (m)	Recovery (%)	Top of recovered core CSF-A (m)	Bottom of recovered core CSF-A (m)	Date (2015)	Time UTC (h)
359-U1469A-										
1R	0.0	5.6	5.6	0.00	0.00	0	0.0	0.00	13 Nov	1345
2R	5.6	15.3	9.7	0.00	0.00	0	5.6	5.60	13 Nov	1430
3R	15.3	25.0	9.7	0.00	0.00	0	15.3	15.30	13 Nov	1525
4R	25.0	34.8	9.8	0.17	0.17	2	25.0	25.17	13 Nov	1600
5R	34.8	44.5	9.7	0.00	0.00	0	34.8	34.80	13 Nov	1640
6R	44.5	54.2	9.7	0.07	0.07	1	44.5	44.57	13 Nov	1710
7R	54.2	63.9	9.7	0.00	0.00	0	54.2	54.20	13 Nov	1730
8R	63.9	73.6	9.7	0.06	0.06	1	63.9	63.96	13 Nov	1750
9R	73.6	83.3	9.7	0.10	0.10	1	73.6	73.70	13 Nov	1820
10R	83.3	93.0	9.7	0.11	0.11	1	83.3	83.41	13 Nov	1835
11R	93.0	102.7	9.7	0.50	0.50	5	93.0	93.50	13 Nov	1920
12R	102.7	112.4	9.7	0.28	0.28	3	102.7	102.98	13 Nov	1955

Table T1 (continued).

Core	Top of cored interval DSF (m)	Bottom of cored interval DSF (m)	Interval advanced (m)	Recovered length (m)	Curated length (m)	Recovery (%)	Top of recovered core CSF-A (m)	Bottom of recovered core CSF-A (m)	Date (2015)	Time UTC (h)
13R	112.4	122.1	9.7	0.18	0.18	2	112.4	112.58	13 Nov	2100
14R	122.1	131.8	9.7	0.38	0.38	4	122.1	122.48	13 Nov	2220
15R	131.8	141.6	9.8	0.00	0.00	0	131.8	131.80	13 Nov	2320
16R	141.6	151.4	9.8	0.26	0.26	3	141.6	141.86	13 Nov	2340
17R	151.4	161.1	9.7	2.03	2.03	21	151.4	153.43	14 Nov	0130
	Hole U1469A totals:		155.5	4.14	4.14					
359-U1469B-										
11	0.0	122.0		*****Drilled from 0.0 to 122.0 mbsf*****					14 Nov	0855
2R	122.0	131.8	9.8	0.30	0.30	3	122.0	122.30	14 Nov	0915
3R	131.8	141.6	9.8	0.10	0.10	1	131.8	131.90	14 Nov	0945
4R	141.6	151.4	9.8	0.32	0.32	3	141.6	141.92	14 Nov	1020
	Hole U1469B totals:		151.4	0.72	0.72					

peared that this hole would be considerably better than the previous hole. This optimism was short lived, as the same hole cleaning problems occurred again after cutting just three RCB cores to 151.4 mbsf. Convinced that the hole could not be deepened any further because of lost circulation, Hole U1469B was also abandoned (see Figure **F1** in the Expedition 359 summary chapter [Betzler et al., 2017b]). The drill string was retrieved back on board, the positioning beacon was picked up, thrusters were raised, and we started the transit to the next site (U1470) at 2045 h on 14 November. Total core recovered in Hole U1469B was 0.72 m (2%) in three RCB cores (Table **T1**).

Lithostratigraphy

Site U1469 was drilled through a succession of hemipelagic deposits into the Kardiva platform. This isolated platform has been described by Beloposky and Droxler (2004), Betzler et al. (2013), and Lüdmann et al. (2013) as an aggrading to prograding platform that developed in the early Miocene, flourished in the middle Miocene, and drowned in the late middle Miocene.

Poor recovery was a significant limitation at this site. The use of the RCB system resulted in very low recovery of the loose sediments forming the upper lithostratigraphic units (I and II). Intense karstification of the lithified carbonate platform facies (Unit III) added additional complications to drilling operations, resulting in lost circulation and abandonment of the hole. In spite of low recovery (Hole U1469A = 2.2%; Hole U1469B = 1.1%), three lithostratigraphic units were defined based on visual core descriptions and thin section analysis and by combining the lithostratigraphy in Holes U1469A and U1469B (Figure **F2**):

Unit I: planktonic foraminifer-rich grainstone.
Unit II: bioclastic grainstone/packstone.
Unit III: dolomitized coral-rich rudstone/floatstone.

Lithostratigraphic units

Unit I

Interval: 359-U1469A-1R-1, 0 cm, to 10R-CC, 7 cm
Depth: 0–93.0 mbsf

Only 22 cm of core was recovered from Unit I, consisting of partly lithified to lithified gray-brown to pale yellow coarse-grained grainstone. Planktonic foraminifers, the dominant constituent, are abundant. Other skeletal grains such as benthic foraminifers, pteropods, echinoderm spines, bryozoan fragments, bivalves, and yellow-red–stained lithoclasts are common. Rare bryozoan and red algae fragments are also present.

Unit II

Intervals: 359-U1469A-11R-1, 0 cm, to 16R-CC, 25 cm; 359-U1469B-1R-1, 0 cm, to 4R-CC, 10 cm
Depth: 93.0–141.70 mbsf

Poor preservation of skeletal grains is one of the main arguments to separate this interval from Unit I, as is the appearance of *Halimeda* fragments and other shallow-marine biota (Figure **F3A**). Unit II consists of lithified medium- to coarse-grained pale yellow, mixed bioclastic grainstone to rudstone. Whole and fragmented bivalves, benthic foraminifers, *Halimeda* fragments, and echinoderm spines are common, and unidentified skeletal grains are abundant. Planktonic foraminifers, bryozoans, and red algae are also present as minor components. The unit fines upward to Unit I. Bioclasts (e.g., planktonic foraminifers) display pervasive overgrowth of calcite cements (Figure **F3B**).

Unit III

Intervals: 359-U1469A-17R-1, 0–21 cm; 359-U1469B-4R-CC, 10–31 cm
Depth: 141.7–153.4 mbsf

The contact between Units II and III occurs between Sections 359-U1469A-16R-CC, 25 cm, and 17R-1, 0 cm (151.40 mbsf). In Hole U1469B, the contact between Unit II and II was recovered in Section 4R-CC, 10 cm. Core 359-U1469A-17R penetrated through the same depth intervals as Core 359-U1469B-4R but did not recover the top carbonate platform boundary at the same location; therefore, the boundary is placed at the first occurrence in Hole U1469A at 141.7 mbsf. This sharp boundary has a distinct color change from very pale brown to pale brown and a lithologic change from coarse-grained grainstone/rudstone to underlying dolomitized floatstone with abundant corals, bivalves, and large benthic foraminifers (Figure **F4**).

Unit III consists of grayish brown lithified granule-grained dolomitized coral-rich floatstone with a very fine grained dolomitic matrix. The main components of this succession are abundant red algae, coral fragments (massive and branching), and encrusting for-

Figure F2. Lithostratigraphic summary, Site U1469.

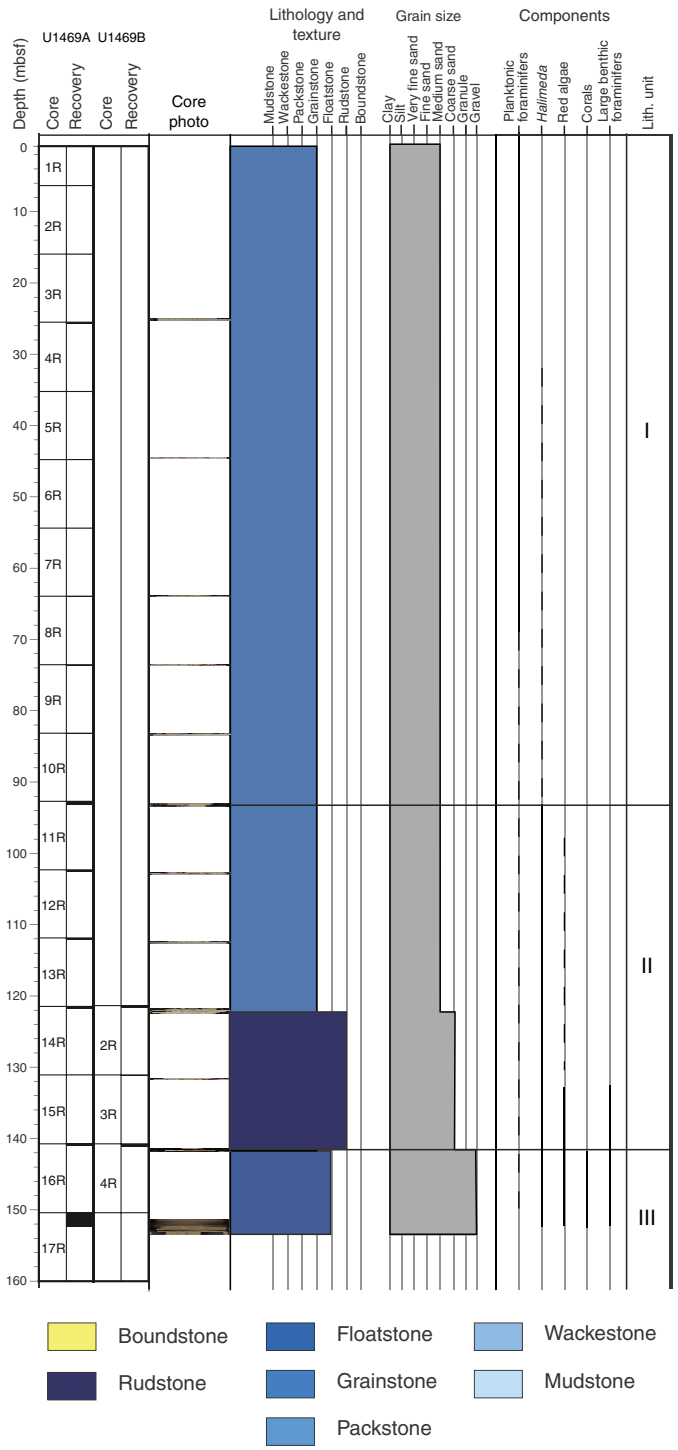

aminifers. Bivalves and gastropods are common to abundant but commonly only preserved as molds. Benthic foraminifers and rhodoliths are present. The top of the unit has borings indicative of a hard substrate that suggests postdeposition lithification and bioerosion (Figure **F5A**). Moldic porosity is pervasive with abundant bioclasts, including bivalves, corals, and green algae being dissolved. Crystals with botryoidal-like geometries were observed on the walls of the molds. Fine crystals of dolomite are present as well-

Figure F3. Bioclastic grainstone. A. Bioclastic grainstone from Unit II (359-U1469B-2R-CC, 3–6 cm; plane-polarized light [PPL]). 1 = *Halimeda* fragments. B. Bioclastic grainstone characteristic of Unit II (359-U1469A-11R-CC, 13–15 cm; PPL). 2 = calcite overgrowth cements on planktonic foraminifers.

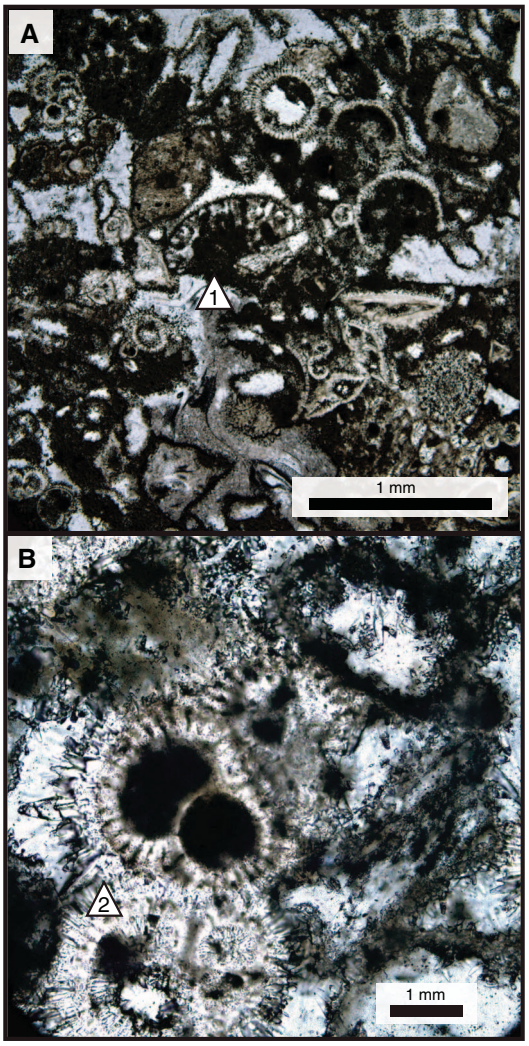

developed large euhedral dolomite crystals (Figure **F5B**), which are responsible for the color change observed between Units II and III. Petrographic analysis shows euhedral rhombs of dolomite crystals that vary between 100 and 50 µm in size, are tightly packed, and form the matrix (Figure **F6**).

Discussion

The overall succession is formed of three lithostratigraphic units; however, two depositional regimes are recognized. The first is a current-driven depositional system that includes Units I and II. The second is a shallow-marine environment dominated by reef-builder organisms on the margin of the isolated carbonate platform.

The coarse-grained, very well sorted grainstones of Unit I represent the youngest hemipelagic deposits and are partly lithified to lithified and gray-brown to pale yellow in color. Similar deposits are observed in the present-day Kardiva Channel, representing current deposits. Bioclasts are typical open-marine pelagic fauna and a very minor proportion of skeletal benthic fauna that may have originated close to the active atolls and were transported by currents to the in-

Figure F4. Unit II/III boundary (359-U1469B-4R). A. Transition from white foraminiferal rudstone (Unit II) to grayish brown dolomitized floatstone (dolostone) (Unit III). 1 = boring, 2 = coral fragment. B. Bioclastic grainstone with benthic foraminifers (Unit II). C. Dolomitized floatstone (Unit III). 3 = encrusting red algae, 4 = coral fragment.

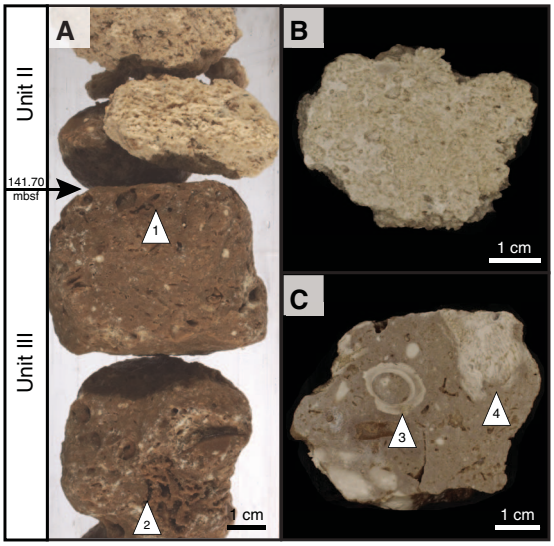

Figure F5. Postdepositional microtexture in Unit III (359-U1469B-4R). A. Dolomitized floatstone (dolostone). 1 = single dolomite rhombs. B. 2 = boring in hard substrate host rock.

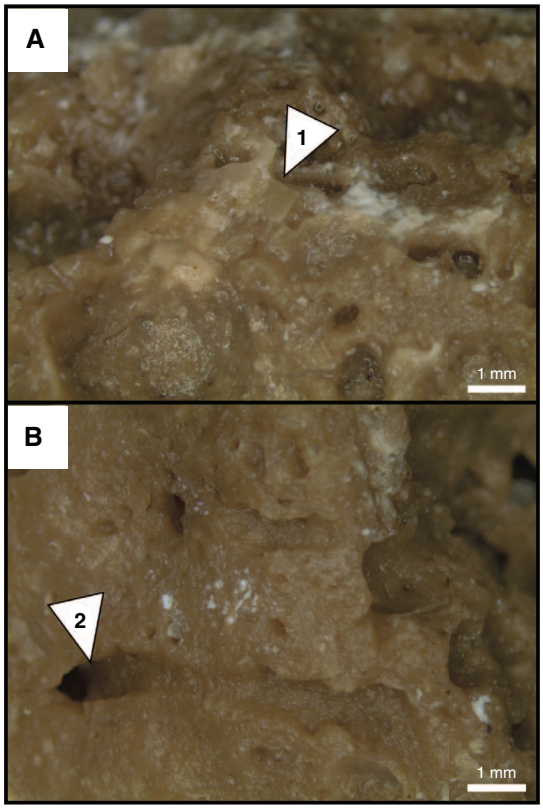

ner channel. The seismic lines and multibeam bathymetry show wave-like geometries (see **Background and objectives**) that are in concert with the interpretation of a drift depositional system for Unit I.

Figure F6. Tightly packed euhedral dolomite crystals in dolomitized floatstone (dolostone) (359-U1469A-17R-2, 16–18 cm) A. cross-polarized light. B. PPL.

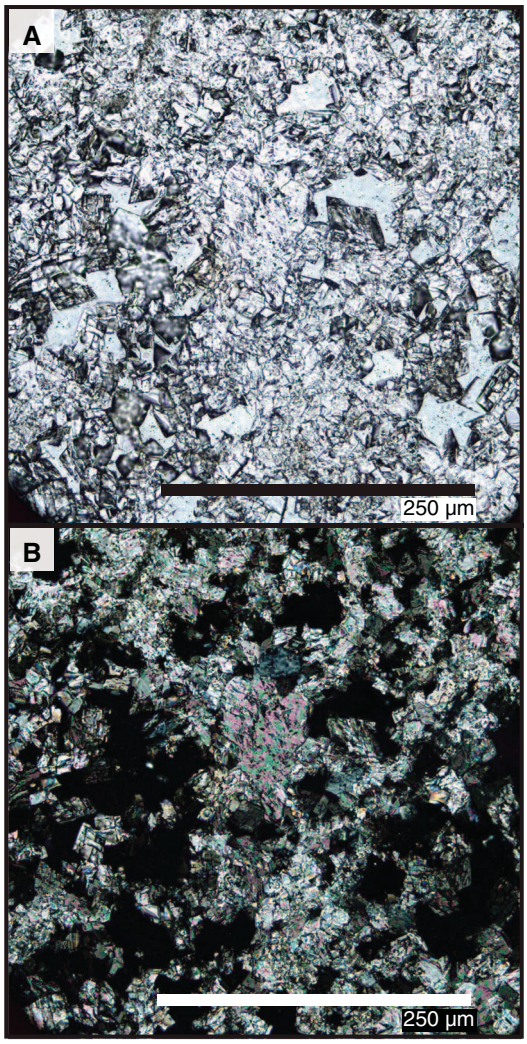

At the base of Unit II, the lithology is composed of coarse-grained neritic fauna that gradually passes into a mix of shallow-marine and open pelagic fauna that clearly indicates a deepening-upward trend to Unit I. In addition, bioclast overgrowth is significant, especially of planktonic foraminifers, due to oversaturated water flux through highly porous deposits (Swart, 2000).

The Unit II/III boundary is hardground. This type of surface represents a hiatus in sedimentation that with time resulted in cementation on the top of the carbonate platform (e.g., Taylor and Wilson, 2003; Tucker, 2003) (Figure **F3**). At Site U1469, the hardground is associated with the drowning of the platform (Betzler et al., 2009). This type of surface normally contains sessile communities and includes borings (Taylor and Wilson, 2003) like those identified at the top of Unit III (Figure **F4B**).

Unit III is interpreted as a shallow-marine reef to fore-reef depositional setting as evidenced by massive and branching coral fragments, rhodoliths, gastropods, and other encrusting organisms. This facies contains abundant reworked broken reefal material that likely infills the space between reef framework structures. Dolomitization of Unit III was most likely associated with normal seawater flux through shallow-marine sediments with high permeability,

similar to the deposits of the Marion Plateau platform and the Bahamas. Such a dolomitization process requires high water–rock interaction and extensive subsurface circulation (e.g., Whitaker et al., 1994; Swart and Melim, 2000; Ehrenberg et al., 2006).

Biostratigraphy

A ~153 m thick sequence was recovered at Hole U1469A that includes the drift succession and the top part of the ancient carbonate platform (see **Lithostratigraphy**). The recovery of Hole U1469B starts at ~122 mbsf and reaches ~141 mbsf within the ancient carbonate platform. Recovery at this site was poor because the RCB coring system did not recover the porous and friable carbonate rocks. Therefore, a continuous record of core catchers was not obtained, hampering the construction of a good biostratigraphic model for this site. In the top part of the sequence, planktonic foraminifers are abundant, with moderate to good preservation. Below Sample 359-U1469A-8R-CC (63.96 mbsf), planktonic foraminifers are rare, or the samples are even barren, and preservation is poor. Nannofossils are sparse with poor preservation. Benthic foraminifers and ostracods were studied in selected samples to evaluate paleoenvironmental conditions, but the preservation of those microfossils is also poor below ~63 mbsf, with intense cement overgrowth. Based on the absence of radiolarians at previous sites, we did not expect to find them at this site either; hence, core catcher samples were not prepared for the study of these microfossils (Figure **F7**).

Calcareous nannofossils

Only very sparse nannofossil assemblages were found in Hole U1469A samples. Assemblages were not datable; however, the presence of small *Gephyrocapsa* specimens in the upper part of the sequence (Samples 359-U1469A-4R-CC, 6R-CC, 8R-CC, 9R-CC, and 10R-CC) indicates that these samples are Quaternary to middle Pliocene in age (Zones NN21 to NN14). Similarly, the consistent presence of *Sphenolithus* specimens in the lower part of the hole (Samples 9R-CC, 10R-CC, 13R-CC, 14R-CC, and 16R-CC) suggests that this part of the sequence is middle Pliocene or older (Zone NN15 or older), although they could be reworked. Given the very poor nature of the assemblages, no Miocene marker species were observed. The two samples available from Hole U1469B (2R-CC and 3R-CC) are barren. Details of the assemblages present are given in Table **T2**.

Planktonic foraminifers

Planktonic foraminifers were examined in core catcher samples from Holes U1469A (10 samples) and U1469B (2 samples). Planktonic foraminifers are abundant at the top of the sequence with moderate to good preservation. Below Sample 359-U1469A-8R-CC (63.96 mbsf), planktonic foraminifers become rare or absent and are difficult to identify because of their poor preservation and calcite overgrowth.

Two Pleistocene biohorizons were identified: the last occurrences (LOs) of *Globigerinoides fistulosus* (1.88 Ma) between Samples 4R-CC (25.17 mbsf) and 6R-CC (44.57 mbsf) and *Globorotalia limbata* (2.39 Ma) between Samples 6R-CC (44.57 mbsf) and 8R-CC (63.96 mbsf). The Pliocene LO of *Dentoglobigerina altispira* (3.47 Ma) was found at the same level as the LO of *G. limbata*, which may be due to the low resolution of the study and the lack of samples from Core 7R. Within the Pliocene, we also identified the LO of *Globorotalia margaritae* between Samples 8R-CC (63.96 mbsf) and 9R-CC (73.7 mbsf) (Tables **T3**, **T4**).

Figure F7. Biostratigraphic and paleoenvironmental summary, Site U1469. Calcareous nannofossil and planktonic foraminifer biozonation is shown with paleoenvironmental information provided by benthic foraminifers and ostracods.

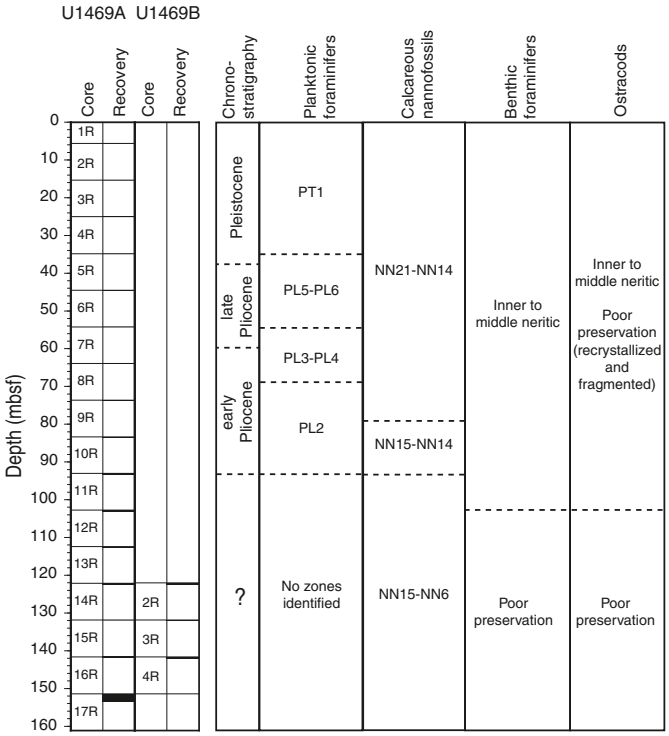

Table T2. Nannofossil range chart, Hole U1469A. **Download table in .csv format.**

Table T3. Biostratigraphic events, Site U1469. LO = last occurrence. PF = planktonic foraminifer. Ages are based on Gradstein et al. (2012). See Raffi et al. (2006) for a review of nannofossil events and original sources for correlations to magnetostratigraphic timescales. **Download table in .csv format.**

Event	Fossil group	Age (Ma)	Age reference	Core, section, interval (cm) last sample above event	Core, section, interval (cm) first sample below event	Top depth (mbsf)	Bottom depth (mbsf)	Midpoint depth (mbsf)
				359-U1469A-	359-U1469A-			
LO *Globigerinoides fistulosus*	PF	1.88	Lourens et al. (2004)	4R-CC	6R-CC	25.17	44.57	34.87
LO *Globorotalia limbata*	PF	2.39	Lourens et al. (2004)	6R-CC	8R-CC	44.57	63.96	54.265
LO *Dentoglobigerina altispira*	PF	3.47	Lourens et al. (2004)	6R-CC	8R-CC	44.57	63.96	54.265
LO *Globorotalia margaritae*	PF	3.85	Lourens et al. (2004)	8R-CC	9R-CC	63.96	73.70	68.83

Table T4. Planktonic foraminifer range chart, Holes U1469A and U1469B. **Download table in .csv format.**

Table T5. Benthic foraminifer range chart, Holes U1469A and U1469B. **Download table in .csv format.**

Benthic foraminifers

Ten core catcher samples were investigated for benthic foraminifers in Hole U1469A, along with two core catcher samples from Hole U1469B. The top of the drift succession of Hole U1469A spans the early Pliocene to Pleistocene and ranges from very good to good preservation. Benthic foraminifers within this interval include specimens of *Calcarina* sp., *Discogypsina* sp., and *Amphistegina* sp. exported from the nearby shallow-water areas. Preservation at the top of the ancient carbonate platform below Sample 359-U1469A-11R-CC becomes very poor, with all foraminifers showing calcite overgrowth. Identification of almost all benthic foraminifers from the two Hole U1469B core catcher samples is difficult due to strong overgrowth on specimens. Echinoderm spine fragments are common (also with overgrowth) throughout Hole U1469B, and large pink dolomite crystals start to appear in the sediment below Sample 8R-CC (Table **T5**).

Ostracods

Ostracods are rare in the core catcher samples from Hole U1469A with only a few valves of Bairdiids and Loxoconchiids found in Samples 4R-CC and 8R-CC to 10R-CC. Both ostracod groups are characteristic of shallow-water marine environments.

Geochemistry

Interstitial water chemistry

At Site U1469, no interstitial water (IW) samples were obtained because of poor recovery.

Bulk sediment geochemistry

Calcium carbonate and organic matter

Calcium carbonate content was determined for seven samples from Cores 359-U1469A-11R through 17R. Carbonate content varies between 95 and 98 wt% (Figure **F8**; Table **T6**).

Total organic carbon (TOC) concentrations were measured on seven samples from the same sections where calcium carbonate was determined and range between 0.04 and 0.15 wt% (Figure **F9**; Table **T6**). Sample 17R-1, 52–54 cm, has calculated TOC of less than zero. This value is an artifact of the inadequate method of determining the amount of organic carbon in carbonate-rich sediments (see **Geochemistry** in the Expedition 359 methods chapter [Betzler et al., 2017a]). All data are included in Table **T6**, but negative values are omitted from Figure **F9**. Total nitrogen ranges between 0.08 and 0.10 wt%.

X-ray diffraction

Mineralogy was determined using X-ray diffraction (XRD) at a rate of approximately one sample per core. In the absence of whole-round squeeze cakes, XRD analyses were performed on splits from the headspace samples.

The mineralogy consists of aragonite, high-Mg calcite (HMC), low-Mg calcite (LMC), and dolomite (Figure **F10**; Table **T7**). High-Mg calcite is present only to 25.00 mbsf and reaches a maximum of

Figure F8. Carbonate content, Site U1469. Horizontal dotted line = depth of the drowned platform top (141.7 mbsf) as identified in Hole U1469B.

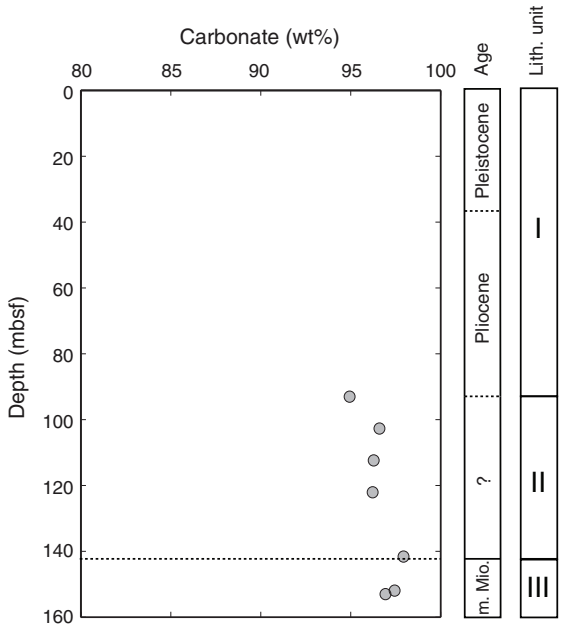

Table T6. Carbon and nitrogen, Site U1469. **Download table in .csv format.**

Figure F9. Organic carbon and nitrogen concentrations, Site U1469. Horizontal dotted line = depth of the drowned platform top (141.7 mbsf) as identified in Hole U1469B. TN = total nitrogen.

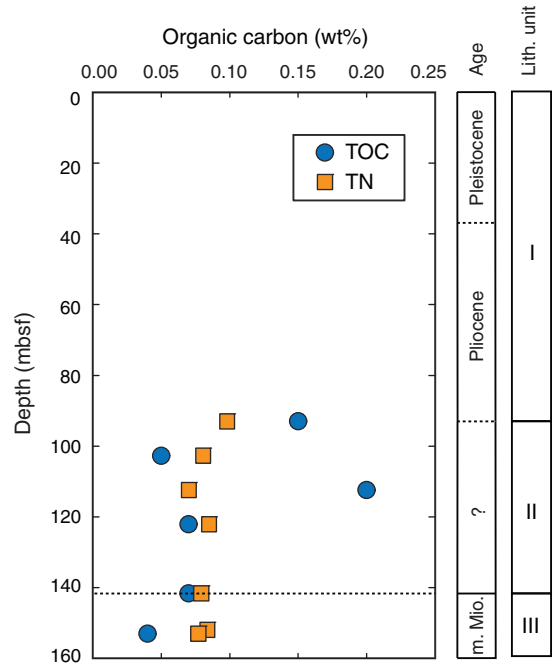

8.9%. Aragonite concentrations are between 10.7% and 49.0% from the surface to 73.6 mbsf. Below this depth, aragonite content decreases to 7%–16.4%. Dolomite concentrations are <3.3% above 93.00 mbsf. Below 93 mbsf, dolomite increases to between 4.4% and

Figure F10. Relative concentrations of aragonite, HMC, LMC, dolomite, and quartz measured using XRD, Site U1469. Horizontal dotted line = depth of the drowned platform top (141.7 mbsf) as identified in Hole U1469B.

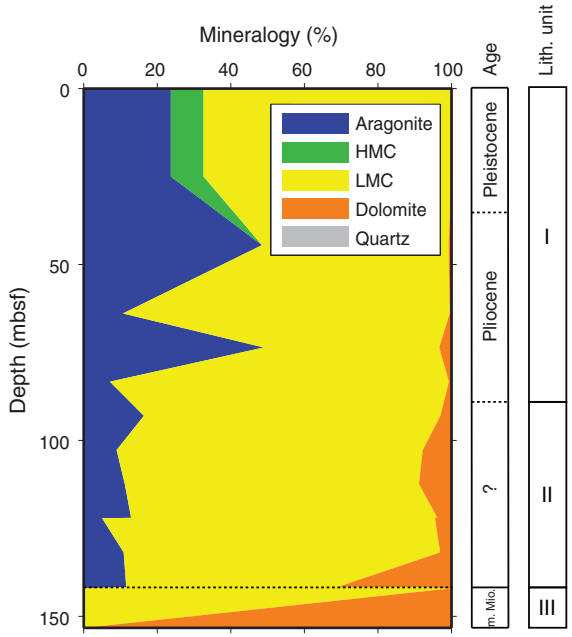

Table T7. XRD results, Site U1469. **Download table in .csv format.**

Table T8. Solid geochemistry, Site U1469. **Download table in .csv format.**

Figure F11. Mg/Ca, Sr/Ca, Mn/Ca, and Fe/Ca ratios of sediments, Site U1469. Horizontal dotted line = depth of the drowned platform top (141.7 mbsf) as identified in Hole U1469B.

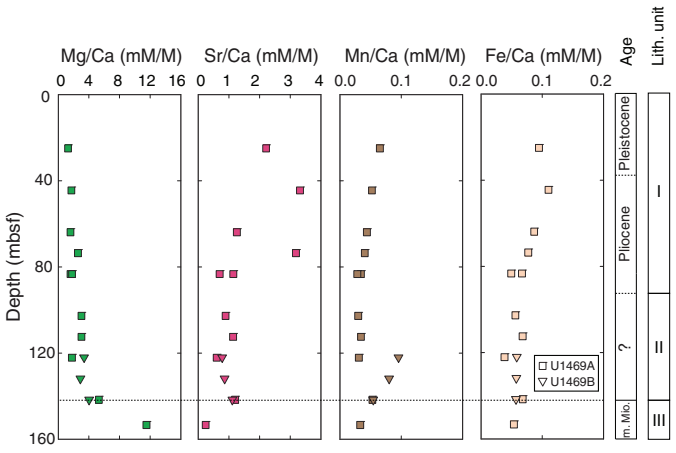

Figure F12. Methane concentrations in headspace samples, Site U1469. Horizontal dotted line = depth of the drowned platform top (141.7 mbsf) as identified in Hole U1469B.

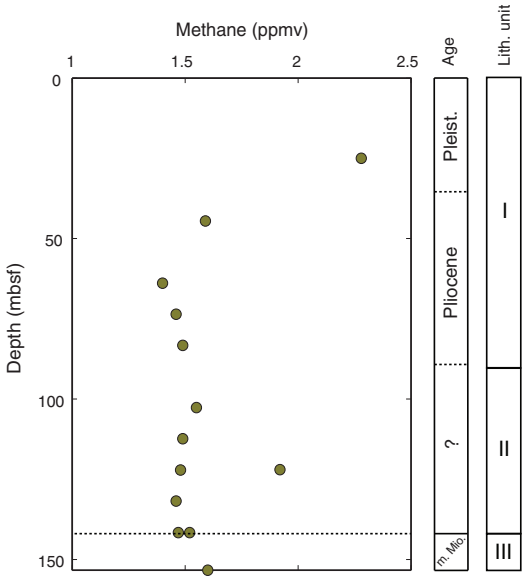

Table T9. Headspace hydrocarbons, Site U1469. **Download table in .csv format.**

30.9% and aragonite content decreases. At 153.22 msbf, the sample is completely dolomitized. Quartz is often observed in the XRD spectra but is never a significant component of the sediments (<1%).

Major, minor, and trace element composition

Minor and trace element composition are presented in Table **T8**, with the most important elements relevant to carbonate diagenesis (Mg, Sr, Fe, and Mn) shown in Figure **F11** as molar ratios relative to calcium.

Ratios of Mg/Ca have baseline values around 1–5 mmol/mol and rise to 11.52 mmol/mol in the deepest core (153.22 msbf). Ratios of Sr/Ca are high (1.26–3.32 mmol/mol) above 80 mbsf. Below that depth, they decrease to <1.2 mmol/mol. Ratios of Mn/Ca are between 0.028 and 0.096 mmol/mol, and Fe/Ca ranges between 0.038 and 0.110 mmol/mol.

Volatile hydrocarbons

Headspace samples for the analysis of methane, ethene, ethane, propene, and propane were obtained from 14 core catchers. Methane concentrations remain low between 1.40 and 2.28 ppmv (Figure **F12**; Table **T9**). No heavier hydrocarbons (C_{2+}) were detected.

Discussion

Carbonate diagenesis

Aragonite is present throughout the Pleistocene and Pliocene (from the sediment surface to 73.6 mbsf) at an abundance similar to those found at Sites U1465 and U1466. These variations reflect input from the adjacent platform during changes in sea level, similar to Site U1466.

Below 73.6 mbsf, most of the aragonite and all of the HMC has neomorphosed to LMC. Dolomite is most abundant in the platform facies. Similar to Sites U1465 and U1466, these changes are interpreted as reflecting diagenetic processes that evolved in response to the prolonged break in sediment production after the platform demise.

The patterns of carbonate diagenesis shown in the carbonate mineralogy are mirrored closely by the sedimentary composition. The high Sr/Ca ratio above 80 mbsf is coincident with the high aragonite content. The dolomite peaks (153.22 mbsf) from XRD are consistent with maxima in sedimentary Mg/Ca ratios.

Origin of organic matter

Carbon/nitrogen (C/N) ratios were used as a primary indicator of the origin of organic matter. Marine organic matter has C/N ratios of 4–20, whereas continental organic matter has C/N ratios >20 (e.g., Bordovskiy et al., 1965; Hedges et al., 1986; Nakai, 1986; Meyers, 1997). At Site U1469, C/N ratios are <3 (Figure **F13**; Table **T6**), suggesting organic matter with a marine origin, although the contribution of inorganic nitrogen sources and methodological errors are not accounted for.

Figure F13. C/N ratio in organic material, Site U1469. Horizontal dotted line = depth of the drowned platform top (141.7 mbsf) as identified in Hole U1469B.

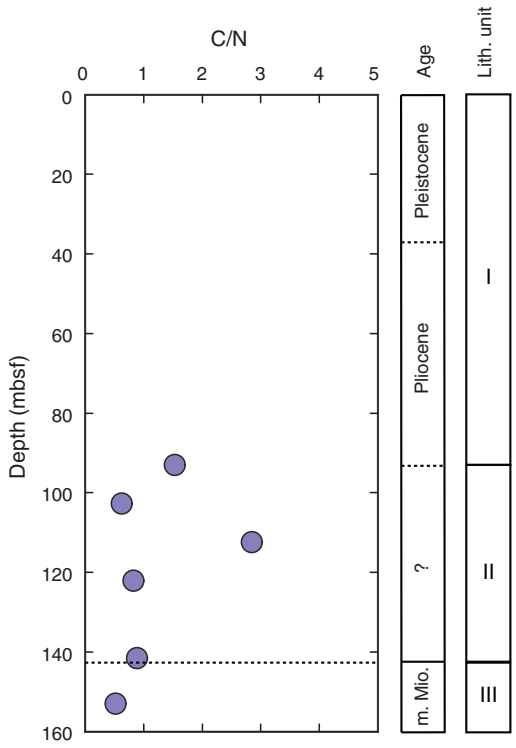

Paleomagnetism

We measured the natural remanent magnetization (NRM) of Sections 359-U1469A-17R-1 and 17R-2 using the superconducting rock magnetometer. These sections were stepwise alternating field demagnetized at 15, 30, and 40 mT. The strong decay of NRM intensity at the 30 mT step shows that the sections were satisfactorily demagnetized. However, intensity does not decay after the 40 mT step, signifying that the magnetic mineral present in this sediment is probably a low-coercivity magnetic mineral (i.e., magnetite). Mean NRM values are 4.14×10^{-3} m/A, and values range from a maximum of 1.17×10^{-2} m/A to a minimum of 8.46×10^{-4} m/A (Figure **F14**). Despite the noisy signal, we were able to tentatively recognize, following the inclination at the 30 mT step, one reversal magnetozone at 153.8 mbsf and a normal magnetozone below. We also recognized a possible short reversal at 153.9 mbsf. Declination changes in those intervals, which supports the possibility that the magnetic signal is driven by geomagnetic changes.

Figure F14. NRM intensity, inclination, and declination, Sections 359-U1469A-17R-1 and 17R-2. Polarity: black = normal, white = reversed.

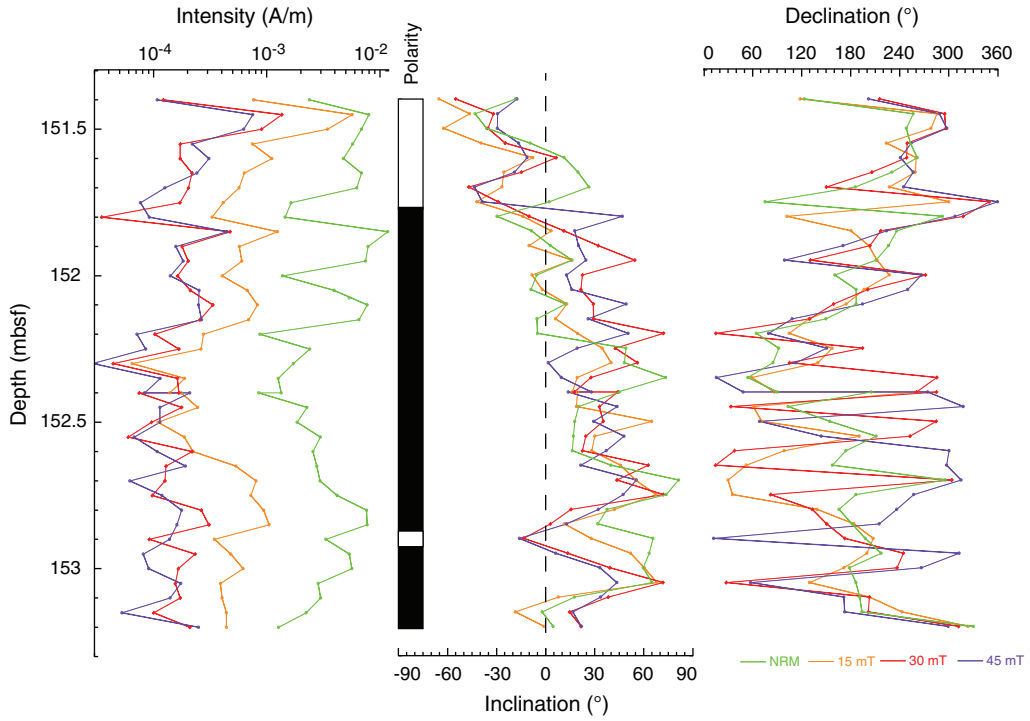

Physical properties

Density, porosity, natural gamma radiation (NGR), color reflectance, magnetic susceptibility (MS), and *P*-wave velocity measurements were performed on Cores 359-U1469A-4R through 17R and 359-U1469B-2R through 4R (~25–154 mbsf). Low recovery yielded a limited number of rock samples that could be analyzed. In addition, thermal conductivity, shear strength, and *P*-wave velocity could not be measured with the Whole-Round Multisensor Logger (WRMSL). *P*-wave velocity was, however, measured using the *P*-wave caliper (PWC) system on discrete cylinder samples and pieces from split cores without liners (Figure **F15**). One density and porosity measurement was taken per core on lithified samples of the drift deposits and the carbonate platform sediments. Physical properties were used to divide the sedimentary succession into two petrophysical (PP) units. Unit 1 ranges from the seafloor to 151.4 mbsf (Cores 359-U1469A-8R through 17R) and corresponds to the Pliocene–Pleistocene drift sediments. Unit 2 consists of two samples covering the carbonate platform limestone and dolomite sediments and shows higher *P*-wave velocity, bulk density, and NGR values compared to those of the drift sediments.

Natural gamma radiation

The two petrophysical units were defined based on the variation in the NGR values (Figure **F15**). In Unit 1, we observed a minor increase in NGR with depth from 2 to 5 counts/s. The limestones and dolostones in Core 17R show a maximum of 40 counts/s. A discrete decrease and increase marks the boundary between Unit 1 and 2.

Density and porosity

Bulk density was measured on whole-round cores with the gamma ray attenuation (GRA) device and on seven discrete samples by moisture and density (MAD) measurements from Cores 359-U1469A-11R through 17R (Figure **F15**). MAD measurements allowed us to calculate grain density and porosity values. In the unlithified sediments of Unit 1, GRA bulk density (1.5–1.8 g/cm^3) and MAD bulk density (1.8–2.0 g/cm^3) show similar trends with an slight offset. The two discrete samples from the carbonate platform (petrophysical Unit 2; lithostratigraphic Unit III) at 153.1 mbsf have high bulk densities of ~2.5 and 2.4 g/cm^3. Grain density remains almost constant in the unlithified sediment strata and varies between 2.8 g/cm^3 at 93 mbsf and about 2.74 g/cm^3 at 142 mbsf. The grain densities of two carbonate platform samples are slightly higher, 2.76 and 2.84 g/cm^3.

Porosity differs strongly between the unlithified and partially lithified drift deposits and the underlying carbonate platform. In the drift sediments, porosity remains relatively constant at 52% but decreases in the last sample to 42%. The two carbonate platform samples have 15.4% and 22.8% porosity, respectively.

P-wave velocity

In the five samples of Unit 1 that were measured, in the unlithified and partially lithified sediments, *P*-wave velocity ranges from 1951 to 2562 m/s, which most likely is related to the high porosity and water content associated with nonlithification or poor lithification of Unit 1 sediments (Figure **F15**). Two PWC samples collected below ~151 mbsf display high velocities of more than 5000 m/s in recrystallized dolomitic intervals of the platform carbonates (see **Lithostratigraphy**).

Color reflectance

L* values decrease from 65 to 24 between 73.6 and 151 mbsf, indicating darker core colors downhole. The variability of L* increases downhole with dark-light color alternations throughout the hole.

Most a* values vary from 2.4 to 10.5 with an overall decrease with depth. Generally, b* gradually increases from approximately –10 to 15 with high variability with depth.

Magnetic susceptibility

Magnetic susceptibility point (MSP or Section Half Multisensor Logger [SHMSL] MS) profiles from 73.4 mbsf (Core 359-U1469A-8R) and magnetic susceptibility loop (MSL or WRMSL MS) profiles from 93 mbsf (Core 11R) to the bottom of the hole in Core 17R show similar trends with a large offset in MSP between about –15 and 0 IU, except for one trough (–135 IU) at 93.1 mbsf, and a large offset in MSL between about –2 to –4 IU. MSP profiles exhibit higher variability.

Discussion

Physical property patterns at Site U1469 are similar to those found at Site U1465 (see **Physical properties** in the Site U1465 chapter [Betzler et al., 2017c]); however, they present remarkable variations in comparison with the drift and carbonate platform sediments of Site U1465 (Figure **F15**). Porosity and grain density in the drift sediments at Site U1469 are lower than those found at Site U1465. Porosity in the carbonate platform sediments at Site U1469 is lower than those at Site U1465, whereas grain density is higher, probably because of differences in lithification and dolomitization. Variations in *P*-wave velocity and porosity most likely reflect differences in lithification and dolomitization that frequently are encountered in the carbonate platforms (Anselmetti and Eberli, 1997).

Figure F15. NGR, bulk density, grain and dry density, porosity, and *P*-wave velocity, Site U1469. Dashed line = top of carbonate platform.

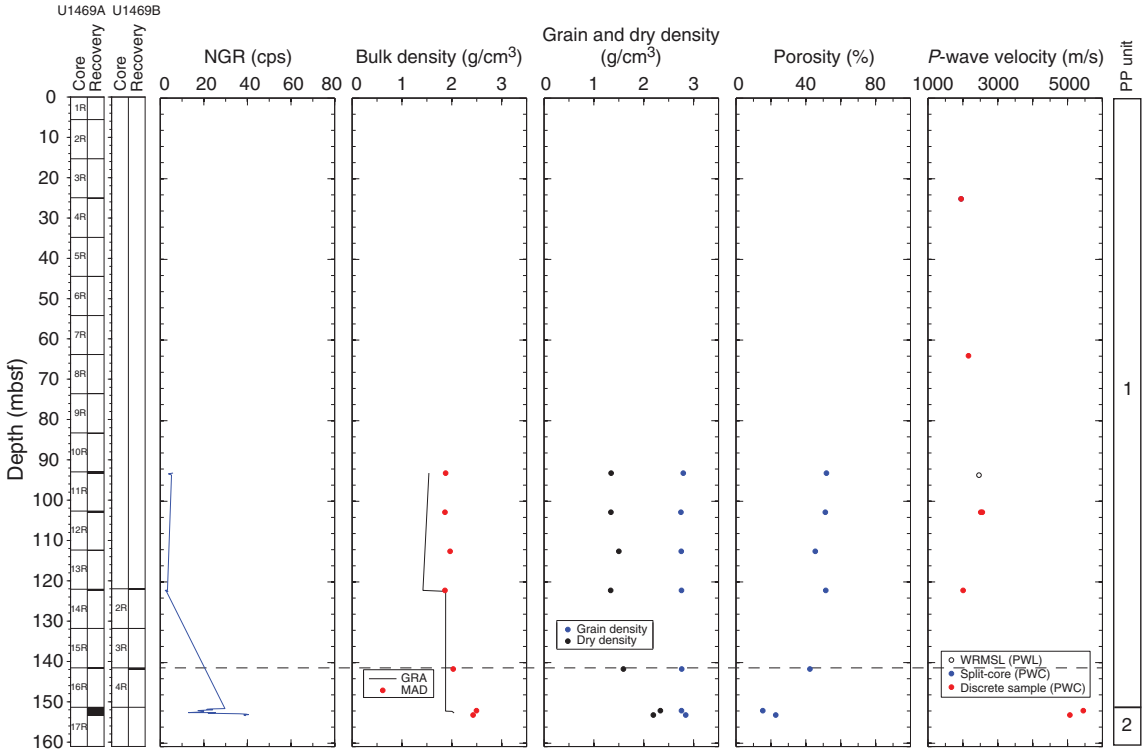

Seismic stratigraphy

Site U1469 is positioned approximately 3 km south of Site U1465 in the western part of the Kardiva Channel close to the Goidhoo atoll (Figure **F1**). Similar to Site U1465, Site U1469 is at the margin of the drowned Kardiva platform that is overlain by drift deposits. At this location, however, sequence stratigraphic interpretation indicates a younger age for the top of the Kardiva platform than the age at Site U1465. In addition, the drift sequences (DS) above DS4 are more complete. This is interpreted as a reflection of the position of the site away from the deepest part of the channel, where the most erosion and stratal condensation occurred. The DS1–DS3 boundaries at Site U1469 are amalgamated into one seismic horizon.

Time-depth conversion

As a result of technical problems with the advanced piston corer (APC)/extended core barrel (XCB) BHA, only RCB drilling was possible at Site U1469, resulting in low recovery in the loose carbonate sands of the drifts above the drowned platform (see **Lithostratigraphy**). Furthermore, unstable hole conditions prevented downhole logging, including a vertical seismic profile. As a consequence, insufficient data were collected to define an internal velocity model at Site U1469. Because of the similarity in geometry and deposition of Site U1469 to those at Site U1465 (see **Lithostratigraphy**), the same velocity model adapted to the corresponding depths was used. Table **T10** lists the computed depth values of the drift sequences and their corresponding two-way traveltimes (TWTs).

Seismic facies and geometries

The seismic facies of the drowned Kardiva platform displays a series of prograding clinoforms with slightly basinward-inclined topsets and steep, sigmoidal foresets that flatten out basinward. Topsets and less inclined foresets consist of high-amplitude reflections, whereas platform edges and steep foresets are low in amplitude (Figure **F16**). In contrast to the platform location at Site U1465, no erosion of the platform top is visible, but an additional thin platform sequence (PS11) with a strong top reflection onlaps the underlying clinoform. This last sequence and the underlying margin and foresets were the target for coring at Site U1469. The drowned platform (PS11) is onlapped by DS1–DS3 and overlain by

Table T10. Drift sequence boundaries, Site U1469. **Download table in .csv format.**

Sequence (bottom)	TWT (ms)	Depth (mbsf)
DS10	34.5	25
DS9	56	38
DS8	95	64.5
DS7	98.5	77.5
DS6	117	93
DS5	135	107.5
DS1–DS4	169	141.5

Figure F16. Seismic section of the drowned Kardiva platform overlain by drift deposits, Site U1469. DS1 (dark blue) marks the base of the current-controlled sedimentation in the Inner Sea.

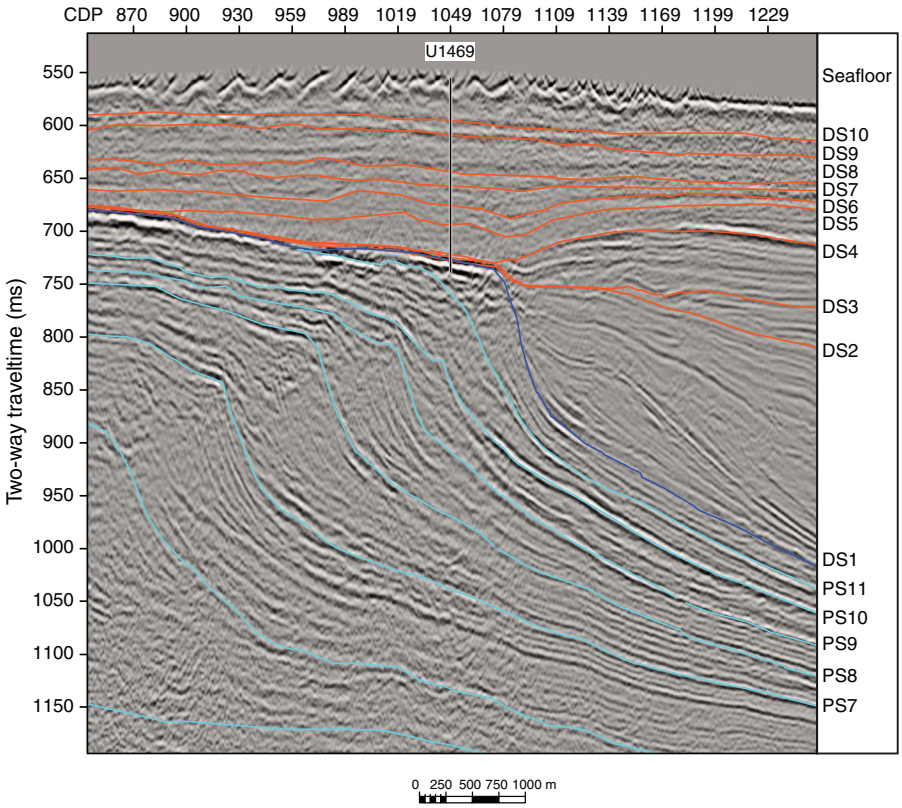

Figure F17. Correlation of seismic and core data, Site U1469. Seismic Line 32 (SO236) is shown with the platform and drift sequences. The few recovered rocks yielded some bulk density information. Interval velocity profile is taken from Site U1465.

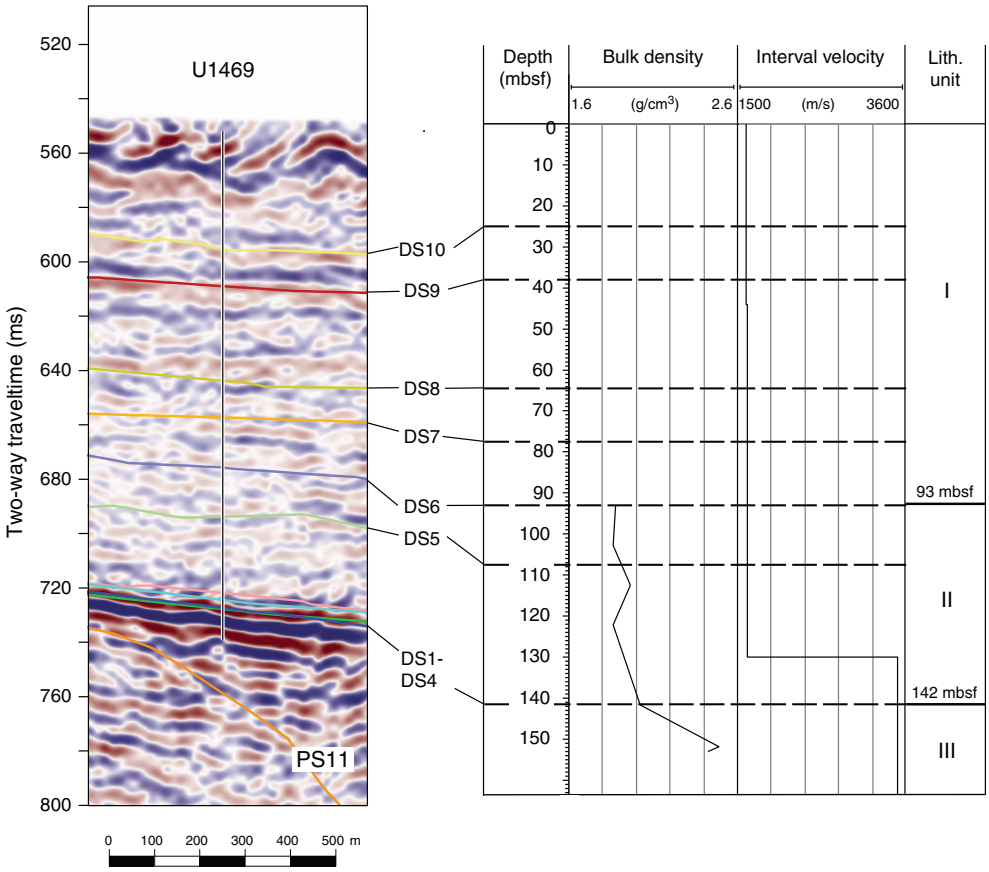

DS4–DS10, which contain low- to medium-amplitude reflections (Figures **F16**, **F17**).

Core-seismic correlation

Bit drops and lost circulation in the top few meters of the platform prevented coring the margin of PS11 and the underlying foresets. The few pieces of rock recovered from the drowned platform, however, confirm that the platform top is represented by well-lithified dolostone. This lithology is in line with the high acoustic impedance contrast between the platform and the overlying drifts (i.e., limestone and loose planktonic foraminiferal sands).

References

Anselmetti, F.S., and Eberli, G.P., 1997. Sonic velocity in carbonate sediments and rocks. *In* Palaz, A., and Marfurt, F.J. (Eds.), *Geophysical Developments Series* (Volume 6): *Carbonate Seismology.* Thomsen, L.A. (Series Ed.): Tulsa, OK (Society of Exploration Geophysicists), 53–74. **http://dx.doi.org/10.1190/1.9781560802099.ch4**

Belopolsky, A.V., and Droxler, A.W., 2004. Seismic expressions and interpretation of carbonate sequences: the Maldives platform, equatorial Indian Ocean. *AAPG Studies in Geology,* 49. **http://archives.datapages.com/data/specpubs/study49/images/st49.pdf**

Betzler, C., Eberli, G.P., Alvarez Zarikian, C.A., Alonso-García, M., Bialik, O.M., Blättler, C.L., Guo, J.A., Haffen, S., Horozal, S., Inoue, M., Jovane, L., Kroon, D., Lanci, L., Laya, J.C., Ling Hui Mee, A., Lüdmann, T., Nakakuni, M., Nath, B.N., Niino, K., Petruny, L.M., Pratiwi, S.D., Reijmer, J., Reolid, J., Slagle, A.L., Sloss, C.R., Su, X., Swart, P.K., Wright, J.D., Yao, Z., and Young, J.R., 2017a. Expedition 359 methods. *In* Betzler, C., Eberli, G.P., Alvarez Zarikian, C.A., and the Expedition 359 Scientists, *Maldives Monsoon and Sea Level.* Proceedings of the International Ocean Discovery Program, 359: College Station, TX (International Ocean Discovery Program). **http://dx.doi.org/10.14379/iodp.proc.359.102.2017**

Betzler, C., Eberli, G.P., Alvarez Zarikian, C.A., Alonso-García, M., Bialik, O.M., Blättler, C.L., Guo, J.A., Haffen, S., Horozal, S., Inoue, M., Jovane, L., Kroon, D., Lanci, L., Laya, J.C., Ling Hui Mee, A., Lüdmann, T., Nakakuni, M., Nath, B.N., Niino, K., Petruny, L.M., Pratiwi, S.D., Reijmer, J., Reolid, J., Slagle, A.L., Sloss, C.R., Su, X., Swart, P.K., Wright, J.D., Yao, Z., and Young, J.R., 2017b. Expedition 359 summary. *In* Betzler, C., Eberli, G.P., Alvarez Zarikian, C.A., and the Expedition 359 Scientists, *Maldives Monsoon and Sea Level.* Proceedings of the International Ocean Discovery Program, 359: College Station, TX (International Ocean Discovery Program). **http://dx.doi.org/10.14379/iodp.proc.359.101.2017**

Betzler, C., Eberli, G.P., Alvarez Zarikian, C.A., Alonso-García, M., Bialik, O.M., Blättler, C.L., Guo, J.A., Haffen, S., Horozal, S., Inoue, M., Jovane, L., Kroon, D., Lanci, L., Laya, J.C., Ling Hui Mee, A., Lüdmann, T., Nakakuni, M., Nath, B.N., Niino, K., Petruny, L.M., Pratiwi, S.D., Reijmer, J.J.G., Reolid, J., Slagle, A.L., Sloss, C.R., Su, X., Swart, P.K., Wright, J.D., Yao, Z., and Young, J.R., 2017c. Site U1465. *In* Betzler, C., Eberli, G.P., Alvarez Zarikian, C.A., and the Expedition 359 Scientists, *Maldives Monsoon and Sea Level.* Proceedings of the International Ocean Discovery Program, 359: College Station, TX (International Ocean Discovery Program). **http://dx.doi.org/10.14379/iodp.proc.359.103.2017**

Betzler, C., Fürstenau, J., Lüdmann, T., Hübscher, C., Lindhorst, S., Paul, A., Reijmer, J.J.G., and Droxler, A.W., 2013. Sea-level and ocean-current control on carbonate-platform growth, Maldives, Indian Ocean. *Basin*

Research, 25(2):172–196. **http://dx.doi.org/10.1111/j.1365-2117.2012.00554.x**

Betzler, C., Hübscher, C., Lindhorst, S., Reijmer, J.J.G., Römer, M., Droxler, A.W., Fürstenau, J., and Lüdmann, T., 2009. Monsoon-induced partial carbonate platform drowning (Maldives, Indian Ocean). *Geology,* 37(10):867–870. **http://dx.doi.org/10.1130/G25702A.1**

Bordovskiy, O.K., 1965. Transformation of organic matter in bottom sediments and its early diagenesis. *Marine Geology,* 3(1–2):83–114. **http://dx.doi.org/10.1016/0025-3227(65)90005-8**

Ehrenberg, S.N., McArthur, J.M., and Thirlwall, M.F., 2006. Growth, demise, and dolomitization of Miocene carbonate platforms on the Marion Plateau, offshore NE Australia. *Journal of Sedimentary Research,* 76:91–116. **http://dx.doi.org/10.2110/jsr.2006.06**

Gradstein, F.M., Ogg, J.G., Schmitz, M.D., and Ogg, G.M. (Eds.), 2012. *The Geological Time Scale 2012:* Amsterdam (Elsevier).

Hedges, J.I., Clark, W.A., Quay, P.D., Richey, J.E., Devol, A.H., and Santos, U.D., 1986. Compositions and fluxes of particulate organic material in the Amazon River. *Limnology and Oceanography,* 31(4):717–738. **http://dx.doi.org/10.4319/lo.1986.31.4.0717**

Lourens, L., Hilgen, F., Shackleton, N.J., Laskar, J., and Wilson, D., 2004. The Neogene period. *In* Gradstein, F.M., Ogg, J.G., and Smith, A. (Eds.), *A Geologic Time Scale 2004:* Cambridge, United Kingdom (Cambridge University Press), 409–440. **http://dx.doi.org/10.1017/CBO9780511536045.022**

Lüdmann, T., Kalvelage, C., Betzler, C., Fürstenau, J., and Hübscher, C., 2013. The Maldives, a giant isolated carbonate platform dominated by bottom currents. *Marine and Petroleum Geology,* 43:326–340. **http://dx.doi.org/10.1016/j.marpetgeo.2013.01.004**

Meyers, P.A., 1997. Organic geochemical proxies of paleoceanographic, paleolimnologic, and paleoclimatic processes. *Organic Geochemistry,* 27(5–6):213–250. **http://dx.doi.org/10.1016/S0146-6380(97)00049-1**

Nakai, N., 1986. Paleoenvironmental features of Lake Biwa deduced from carbon isotope compositions and organic C/N ratios of the upper 800-m sample of 1, 400-m cored column. *Proceedings of the Japan Academy, Series B: Physical and Biological Sciences,* 62(8):279–282. **http://dx.doi.org/10.2183/pjab.62.279**

Raffi, I., Backman, J., Fornaciari, E., Pälike, H., Rio, D., Lourens, L., and Hilgen, F., 2006. A review of calcareous nannofossil astrobiochronology encompassing the past 25 million years. *Quaternary Science Reviews,* 25(23–24):3113–3137. **http://dx.doi.org/10.1016/j.quascirev.2006.07.007**

Swart, P.K., 2000. The oxygen isotopic composition of interstitial waters: evidence for fluid flow and recrystallization in the margin of the Great Bahama Bank. *In* Swart, P.K., Eberli, G.P., Malone, M.J., and Sarg, J.F. (Eds.), *Proceedings of the Ocean Drilling Program, Scientific Results,* 166: College Station, TX (Ocean Drilling Program), 91–98. **http://dx.doi.org/10.2973/odp.proc.sr.166.130.2000**

Swart, P.K., and Melim, L.A., 2000. The origin of dolomites in Tertiary sediments from the margin of Great Bahama Bank. *Journal of Sedimentary Research,* 70(3):738–748. **http://dx.doi.org/10.1306/2DC40934-0E47-11D7-8643000102C1865D**

Taylor, P.D., and Wilson, M.A., 2003. Palaeoecology and evolution of marine hard substrate communities. *Earth-Science Reviews,* 62(1–2):1–103. **http://dx.doi.org/10.1016/S0012-8252(02)00131-9**

Tucker, M.E., 2003. *Sedimentary Rocks in the Field* (3rd edition): Chichester, United Kingdom (John Wiley & Sons).

Whittaker, F.F., Smart, P.L., Vahrenkamp, V.C., Nicholson, H., and Wogelius, R.A., 1994. Dolomitization by near-normal seawater? Field evidence from the Bahamas. *In* Purser, B., Tucker, M., and Zenger, D. (Eds.), *Dolomites: A Volume in Honor of Dolomieu:* Oxford, United Kingdom (Blackwell Publishing Ltd.), 111–132. **http://dx.doi.org/10.1002/9781444304077.ch8**